

www.acsami.org Research Article

Electrode Effects on Flexible and Robust Polypropylene Ferroelectret Devices for Fully Integrated Energy Harvesters

Juan Pastrana, Henry Dsouza, Yunqi Cao, José Figueroa, Ian González, Juan J. Vilatela, and Nelson Sepúlveda*



Cite This: https://dx.doi.org/10.1021/acsami.0c02019



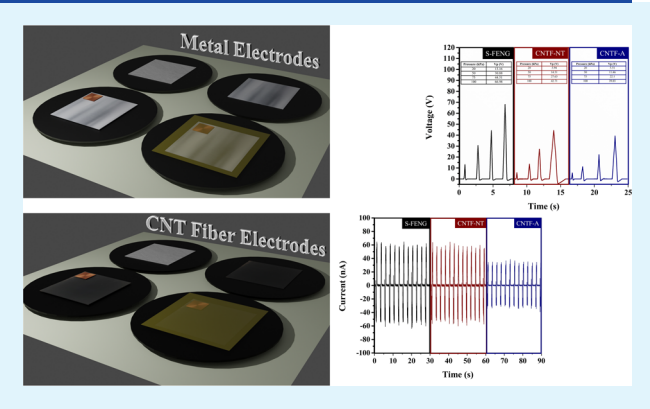
ACCESS

III Metrics & More

Article Recommendations

s Supporting Information

ABSTRACT: This work presents a characterization study of the electrode interface in polypropylene ferroelectret nanogenerators. An emphasis is made on the comparison of carbon nanotube fiber electrodes with traditional metallic thin film electrodes. Multiple experiments were performed on samples with the same electrode dimensions for a range of applied pressures. Results showed higher open-circuit voltage peak values for the thin film metal electrodes, regardless of the applied pressure. Interestingly, the difference in short-circuit current values between metal and carbon nanotube-based fiber electrodes was not as significant. The carbon nanotube fiber electrode was further investigated by post-treating the fiber with acetone and comparing the results with untreated carbon nanotube film electrodes and thin film metal electrodes. In an effort to enable a monolithic integration of ferroelectret energy harvesters with flexible



energy storage elements, this work also presents studies on generation and leakage of induced free charge in the electrodes of flexible ferroelectret energy harvesters. It was found the current leakage through parasitic elements is a faster process than dipole relaxation in the polypropylene film. Finally, an electrode reliability study shows no significant difference in the electrical output of the devices with metallic thin film electrodes after single folding but shows a significant deterioration after crumpling; meanwhile, these processes had no effect on the performance of similar devices with carbon nanotube fiber-based electrodes.

KEYWORDS: ferroelectret, piezoelectric, nanogenerator, flexible, energy harvesting, energy conversion, power management, self-powering

1. INTRODUCTION

Increasing demand on wearable electronics and the rapid progress on piezoelectric thin film materials have inspired growing research interest on the development of self-powered flexible systems. Biocompatible, flexible pressure sensors have been exploited in the field of robotics¹ and health monitoring.² Furthermore, piezoelectric patches can now be attached to plate-like structures in automotive,³ submerged systems,⁴ and aerospace applications,⁵ which enables energy harvesting.⁶ Such applications require devices to be flexible but also robust, with every component being capable of sustaining large deformations such as twisting, folding, bending, and stretching while maintaining their electrical properties. Furthermore, recent efforts have attempted to develop fully monolithic systems, where the energy-harvesting element is integrated with energy storage systems such as supercapacitors.⁷

In the quest for new materials that can perform their electrical functionality while simultaneously having mechanical robustness, carbon-based materials have received plenty of attention. This is mainly due to their ability to offer mechanical flexibility while retaining acceptable conductivity for their use as electrodes. In particular, if axially aligned and highly packed,

carbon nanotube fibers (CNTFs) present higher specific modulus and specific strength than commercial carbon and polymeric fibers. Their constitutional advantages, electrical properties, and particular flexibility enable an adaptability feature that makes them attractive for becoming structural components in a variety of applications such as current collectors, soft robotics, photonics, power generators, supercapacitors, photonics, and energy scavengers.

Nonpolar polymers exhibiting ferroelectric-like behavior when subjected to a high electric field are classified as ferroelectret materials. Ferroelectret are polymer foams, where a gas is injected in the pores of the polymer and is subjected to electrical breakdown by applying a high electric field. As a consequence of the breakdown of the gas, microplasma discharges are formed, and micrometer-scale

Received: February 2, 2020 Accepted: April 28, 2020 Published: April 28, 2020



dipoles are created inside the polymer.^{17,18} Applying a mechanical stress or a temperature change can reshape the polarization of the pores, generating charge accumulation in the electrodes, and an electrical output (i.e., voltage or current) is produced. Ferroelectrets have been used for years in multiple applications including self-powered sensors ^{16,17,19,20} and energy harvesting.²¹ It should be noted that ferroelectrets are, in general, very similar to piezoelectrets, except for the significant different size scale. In fact, ferroelectrets have also been referred to as piezoelectrets in prior work.^{22–25} However, in an effort to distinguish from atomic-scale dipole moment mechanisms, this work refers to polypropylene as a ferroelectret and the device as ferroelectret nanogenerator (FENG).

Although work has been done addressing the integration of energy-harvesting materials for the development of wearable textiles, 26-29 this paper builds on the current need for fundamental research on the characterization of robust, reliable electrodes for electric components in flexible, wearable, monolithically integrated systems. Some recent work along these lines has addressed the integration of ferroelectrets with supercapacitors for the development of wearable textiles. This work is focused on the integration of CNTFs as electrodes in flexible polypropylene ferroelectret films (PPFEs) that have an electric response to a mechanical stimulus. It sheds light on the understanding of the movement of induced charge, particularly at the electrode/supercapacitor interface, which is necessary to control ripple currents from the device to energy storage components and enable fully integrated thin film-based energyharvesting system development. A study that explains the electric behavior of FENG devices when using CNTF-based electrodes is presented. This work targets the characterization of electrodes that requires robustness and flexibility. It has been found that acetone could easily infiltrate into the yarn and fill the interspaces among the CNTs.30 In addition, acetone treatment has been found to reduce the diameter of individual CNTs and increase the Young's modulus of the CNTF.³¹ Thus, the study of acetone treatment of CNTF fibers used as electrodes in FENG devices is also of interest, especially when considering the device's mechanical robustness that can be added by this postprocessing step. In order to have a frame of reference and understand the separate effects of each parameter that are being studied, the performance of both CNTF-based electrodes (before and after acetone treatment) is compared to metal-based electrode counterpart. The device dynamic discharging behavior is studied for a mechanical step input, which is different from the typical mechanical impulses used for electromechanical characterization and lumped model derivation. In addition, the reliability and robustness of the electrodes are studied. In contrast to the interest where cracks are used in electrodes to improve detection in sensors,³² or to enhance mass transport in electrodes,³³ this work focuses on crack-free electrodes which are of importance on assisting FENG devices in their integration with monolithically integrated energy storage systems.

The present research methodology would be expected to be applicable to nanogenerators where the operation principle relies on the accumulated charge due to dipole compression. This would be the case of piezoelectric-based nanogenerators. On the other hand, applying such fiber electrodes to triboelectric-based generators may not be as straightforward since these types of nanogenerators rely on friction as their fundamental working principle (e.g., rubbing two different

materials to generate an electrical output); meanwhile, the present work relies on compression normal to the surface. Since the electrode in this study is a fiber, pilling could become an issue during friction. It should be clarified that this does not mean that fibers could not be used in triboelectric-based nanogenerators. In fact, there is plenty of prior work with remarkable results in triboelectric nanogenerators, where carbon nanotubes have been used as electrodes. However, they do not follow the same fabrication process as the one used in this work; they are either grown *in situ* over the substrate to be used as one of the electrodes,³⁴ or an additional polymer layer is used in combination with the CNTs.³⁵ Some previous works have used cotton threads, but they have treated the material with certain coatings to prevent peeling, in addition to twisting the yarns.^{36,37}

2. RESULTS AND DISCUSSION

The experimental results are discussed next, focusing on open-circuit voltage $(V_{\rm OC})$ and short-circuit current $(I_{\rm SC})$ experiments, separately. The mechanical input for these experiments consisted of a cyclic pressure applied through a computer-controlled piston that resulted in a triangular profile. Applied pressure was calculated by using a force sensor and the dimensions of the device. After $V_{\rm OC}$ and $I_{\rm SC}$ experiments, a study of the dynamics of the generation and leakage of induced charge at the electrodes due to a mechanical step input was done. A detailed description of the materials and devices that are studied can be found in Section 4 (Experimental Section) at the end of this manuscript, where device geometry, fabrication, and abbreviations are fully described. Description on the measurement setup details is provided in the Supporting Information section.

2.1. $V_{\rm OC}$ **Output.** The $V_{\rm OC}$ of a FENG device depends linearly on the magnitude of the applied force (or pressure). Thus, each sample was expected to have a $V_{\rm OC}$ peak value ($V_{\rm p}$) that increases with pressure, which was the observed behavior shown in Figure 1. This experiment was repeated three times for each sample and pressure, and the same behavior was measured. It is observed that, for any given pressure, the measured $V_{\rm p}$ is the largest for the S-FENG sample, and the difference in this value between the two CNT fiber-based FENGs is smaller than the difference between the $V_{\rm p}$ for the S-FENGs is smaller than the difference between the $V_{\rm p}$ for the S-FENGs is smaller than the difference between the $V_{\rm p}$ for the S-FENGs is smaller.

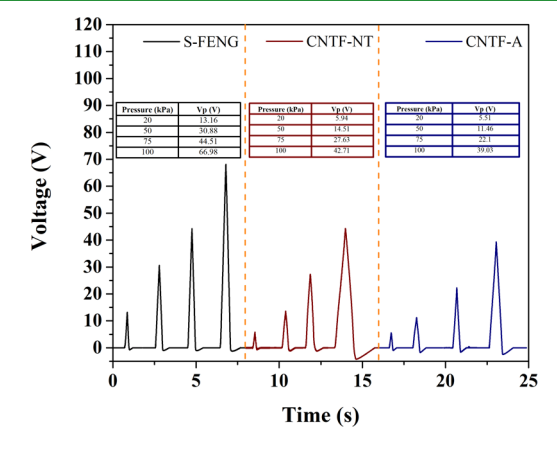


Figure 1. $V_{\rm OC}$ for 20 mm \times 40 mm S-FENG, CNTF-NT, and CNTF-A samples. From left to right, peaks correspond to pressures of 20, 50, 75, and 100 kPa for each sample. The $V_{\rm p}$ values for each corresponding pressure are summarized on the embedded tables.

FENG and CNTF-NT samples. This observation indicates that the difference in conductivity of the three different electrodes may be playing a dominant role in determining $V_{\rm OC}$ since the difference in conductivity between silver and CNTF is about 3 orders of magnitude (($\sigma_{(\text{silver})} \approx 1 \times 10^7 \text{ S/m}$, $\sigma_{(\text{CNTF-NT})} \approx 1 \times 10^7 \text{ S/m}$ 10⁴ S/m), while the difference in conductivity of CNTF after acetone treatment is by a factor of 2 (at most). Thus, these results provide the first demonstration that the CNTF layer can be used as a current collector to transfer charge from piezoelectric energy-harvesting processes. The interest then is in comparing their electrical performance to that of conventional metallic conductors. It is also worth mentioning that, although silver-based devices show higher V_p values, their peak widths and integral values were consistently smaller than those obtained for CNTF-based samples. Noting that the electrical energy produced by each pulse is proportional to the integral of the voltage-current product, this suggests that higher energies can be obtained from the CNTF-based samples.

Another difference between electrodes (in addition to conductivity) relates to the process of transferring the force of the mechanical input to the PPFE film. The applied force by the step motor was computer-controlled through the total displacement of the piston (see the Supporting Information for details). In the present case, the force applied on the electrode becomes a uniform distributed load, which is transferred through the electrode to the surface of the PPFE film, generating compression of the microscaled dipoles across the film's thickness. The force acting on the PPFE surfaces (for any of the different electrodes) can be expressed as $F = \frac{YA\Delta t}{t}$, where Y represents the Young's modulus of the electrode, A is the cross-sectional area, t is the initial thickness of the electrode, and Δt represents the change in the electrode thickness during compression. The samples were actuated using a piston with the same surface area, leaving Y and $\frac{\Delta t}{t}$ as the two parameters that influence the force across the different electrodes. As it is explained next, the former is the dominant factor for the difference in V_p between the S-FENG and the CNT-NT electrodes.

Since the step motor uses a change in the piston's displacement to control the applied force, an electrode with a larger thickness (t) will also show a larger thickness compression (Δt) (see the Supporting Information). It can be shown that an electrode with thickness t_1 that is α times larger than the thickness of another electrode t_2 (e.g., $t_1 = \alpha t_2$, $\forall \alpha > 1$) will have a $\frac{\Delta t}{t}$:

$$\frac{\Delta t_1}{t_1} = \frac{1}{\alpha} \left[(\alpha - 1) + \frac{\Delta t_2}{t_2} \right] \tag{1}$$

In the present case, the thickness of the silver electrodes (\sim 500 nm) is more than 2 orders of magnitude smaller than the thickness of the CNTF-NT electrodes. It should be noted that it would not be accurate to give an exact thickness for the CNTF-based electrodes since the electrode film is very rough and not uniform, with thicknesses up to \sim 100 μ m for CNTF-NT and \sim 10 μ m for CNTF-A (see Section 4). Nevertheless, this thickness variation does not affect the following analysis. The value for $\frac{\Delta t}{t}$ for the samples with CNTF-based electrodes will be larger than for the silver-based counterpart. However, if this parameter dominated, then the force F (and consequently the V_p values) would be larger for CNTF-based samples, which

is opposite to what is measured. Thus, the higher conductivity and larger Young's modulus of silver must be the dominant factors in determining the force applied to the PPFE surface. There is a significant difference between the Young's modulus of CNT fibers (\sim 0.21 GPa for the transverse direction ⁴⁰) and silver (\sim 69 GPa), i.e., $\frac{\gamma_{\rm silver}}{\gamma_{\rm CNTF}} \approx 310$. Although this ratio is not as

large as the largest possible difference in the $\frac{\Delta t}{\epsilon}$ ratio between S-FENG and CNTF-NT samples, there are other physical conditions that need to be taken into consideration. First, it should be noted that the volume occupied by a CNTF-NT electrode contains a large amount of air-filled spaces, unlike a continuous solid film, such as a silver electrode. This effectively reduces further the strain resistance of CNT fiber electrodes. In fact, compression through a thicker, less dense electrode increases compression time, which reflects on the widest measured $V_{\rm OC}$ pulse for the CNTF-NT sample, followed by the CNTF-A sample, which has an electrode thickness and density values between the CNTF-NT and silver electrodes. Second, the much larger roughness of the CNTF electrodes causes a force distribution on the PPFE surface that is less uniform than that of silver, causing dipoles across the film thickness to be compressed at different times and at different rates. Given that $\frac{Y_{\rm silver}}{Y_{\rm CNTF}}$ is much lower than the difference in electrode conductivity, the results suggest a higher charge accumulation at the electrodes when using metal electrodes due to their higher conductivity when compared to CNTF-

When comparing V_{p} between the two CNTF-based FENGs, the difference is not dominated by a difference in conductivity since the relatively small increase in conductivity of CNTF after acetone treatment would be expected to generate an increase in $V_{\rm p}$ (opposite to the observed behavior). $V_{\rm p}$ measurements between the two CNTF-based samples can also be analyzed in terms of the same two parameters: Y and $\frac{\Delta t}{t}.$ However, such analysis would not be as conclusive in this case. Acetone treatment of a CNT fiber results in a reduction of its thickness by a factor of about 50x;³⁹ but at the same time, it makes the film denser by reducing the number of air voids. These two effects induce opposite consequences of similar magnitude on the force F transferred to the PPFE surface. Thus, analyzing these two parameters is not likely to reveal the mechanism for the difference in $V_{\rm p}$ between the two CNTFbased electrodes.

The dominant mechanism for the decrease in V_p in CNTFbased samples after acetone treatment was found after taking a closer look at the cross section of CNTF-A samples in SEM (see Section 4). The PPFE film thickness (d_{PPFE}) was ~30% smaller for CNTF-A samples than for any other sample. This PPFE film thickness reduction also produces a reduction in the average size of the dipoles within the PPFE. Given that $V_{\rm p}$ in FENG devices decreases with the dipole size, 38 it is expected to see smaller V_p values for the samples that were exposed to acetone (CNTF-A electrodes). To further validate this, PPFE samples were treated with acetone and then coated with silver electrodes (hereinafter referred to as S-FENG-A), and the testing of such samples indeed revealed lower V_p values than their counterparts without acetone treatment (see the Supporting Information for V_p measurements on S-FENG-A samples).

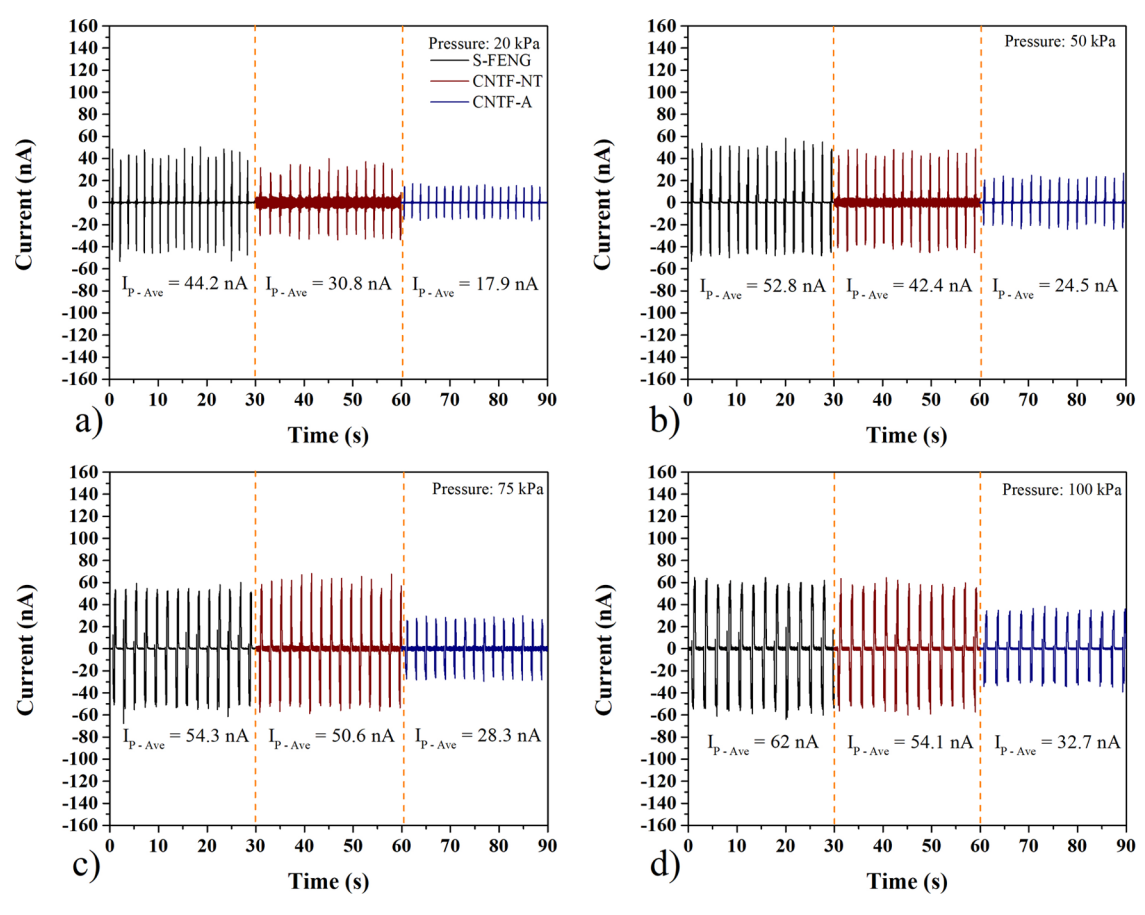


Figure 2. I_{SC} for 20 mm × 40 mm S-FENG, CNTF-NT, and CNTF-A samples at (a) 20, (b) 50, (c) 75, and (d) 100 kPa.

2.2. I_{SC} **Output.** Unlike V_{OC} , I_{SC} curves show a bipolar peak-to-peak response, which has been explained before. ^{38,41} In this work, we use the average of the first I_{SC} peak value (I_{p-ave}) that is produced during the first "pushing" cycle that generated the increasing part of a V_{OC} cycle. It should be noted, however, that both I_{p-ave} values (positive and negative) were very similar, and using either does not change the following analysis and conclusions.

Previous observations suggest that the $I_{\rm SC}$ of a FENG device is determined by the magnitude of the applied force (or pressure) and the rate of change of the applied force, with both contributing similarly for the range of pressures applied in this work (up to 100 kPa). Figure 2 shows that, for the same sample, $I_{\rm p-ave}$ increased as the applied pressure magnitude increased from 20 to 100 kPa (while keeping the same actuation speed). However, this increase is a smaller percentage than the increase in $V_{\rm OC}$ for the same sample and change in pressure. Given that the rate of the applied force was the same for all the samples, these observations suggest that there are additional mechanisms influencing $I_{\rm SC}$, in addition to magnitude and rate of applied pressure.

Electrode conductivity played a role in charge accumulation (i.e., $V_{\rm OC}$), but it would be expected to play an even stronger role in charge flow (i.e., $I_{\rm SC}$). The smaller $I_{\rm p-ave}$ output for the CNTF-based electrodes (when compared to the S-FENG) is most likely due to the smaller conductivity of the CNTF-based electrodes ($\sigma_{\rm (CNTF)} \approx 1 \times 10^4$ S/m; $\sigma_{\rm (silver)} \approx 1 \times 10^7$ S/m). However, electrode conductivity is not the dominant factor for the $I_{\rm SC}$ difference between the samples with CNTF electrodes (which is a higher difference than the one between S-FENG

and CNTF-NT samples) since the conductivity of CNTF is not significantly changed after acetone treatment. The difference in $d_{\rm PPFE}$ between the two CNTF-electrode samples (described earlier) is not the dominant factor either since $I_{\rm SC}$ measurements for S-FENG-A and S-FENG did not show a significant or consistent difference (see the Supporting Information). It is most likely that as a consequence of the densification process due to acetone treatment, the interfacial area between the CNT fiber and PPFE is reduced, relative to the CNTF-NT sample. Still, it happens at the expense of reducing the total contact with the polymer phase.

2.3. Induced Charge: Generation and Leakage. FENG devices have traditionally been studied for mechanical energyharvesting applications, which involves the use of a train of a mechanical "push-pull" cycle input. 38,41,42 Such studies have been used for deriving electromechanical lumped models and to obtain the system's response to typical cyclic pressures found in real applications. 41-43 Cyclic mechanical input was also used in previous sections in this work to describe $V_{\rm OC}$ and I_{SC} for metallic and CNTF-based electrodes. For this type of input, the change in dipole moment during "compression" (i.e., "push" part of the cycle, stage 1 in Figure 3) induces a polarization field across the PPFE dielectric. To balance this field, the system reacts by accumulating induced free charge at each electrode with opposite polarity to the polarization field. If the electrodes are forced to be at the same electric potential (by connecting them together through a short circuit, the ideal case of an ammeter) during the compression process, the induced free charge flows, giving rise to I_{SC} . During decompression (i.e., "pull" part of the cycle), the change in

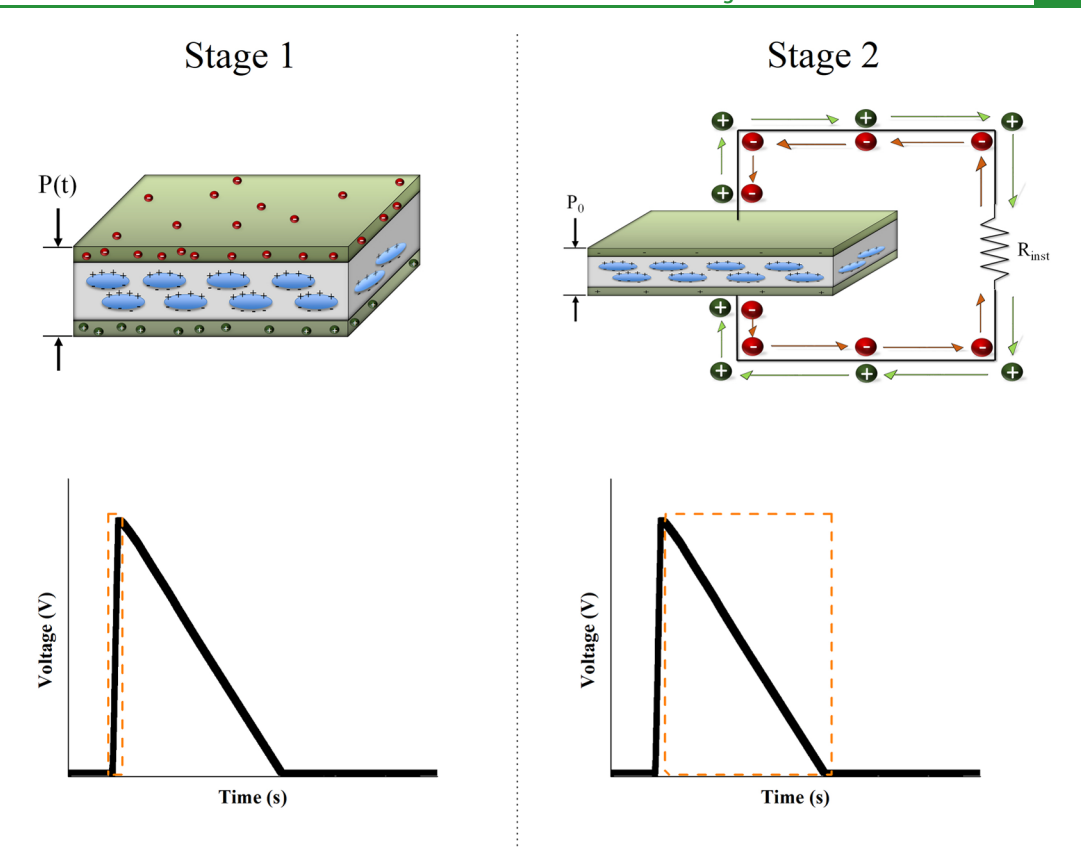


Figure 3. During compression (stage 1), free charge accumulates at each surface to balance the electric potential generated by the displacement field due to dipole moment changes across the PPFE. After the mechanical step input is applied with a pressure P_{o} , surface charge flows slowly in the opposite direction (stage 2). The orange dashed lines on the curves represent the region in the response that corresponds to each stage.

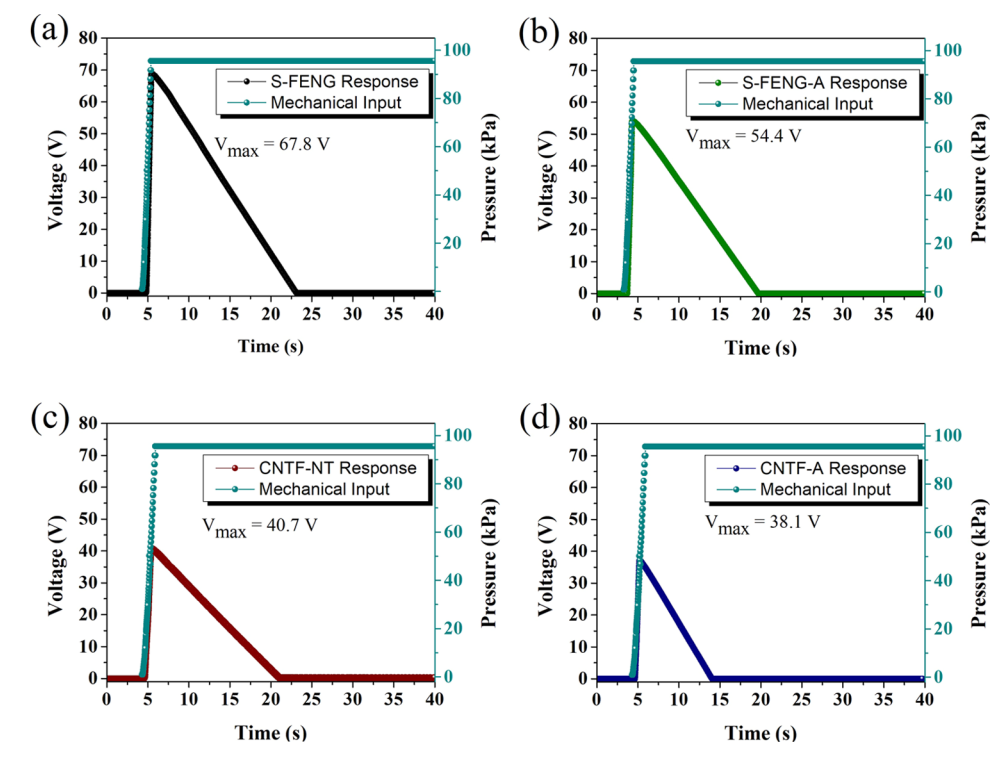


Figure 4. Transient response for 100 kPa for all the samples: (a) S-FENG, (b) S-FENG-A, (c) CNTF-NT, and (d) CNTF-A samples.

the dipole moment flips sign, and the reverse process occurs. The instant when the mechanical input changes from "push" to "pull" cycle, the charge flow also changes direction; crossing

Isc = 0 at the point where the mechanical input changes direction. In terms of electric potential, charge accumulation during compression generates an electric field that is largest at

the end of the compression cycle and returns to zero at the end of the release cycle. Thus, a "push-pull" mechanical cycle results in a "positive—negative" $I_{\rm SC}$ cycle and an "increasing—decreasing" $V_{\rm OC}$ cycle (as shown in Figures 1 and 2).

If FENG devices are to be monolithically integrated with supercapacitors in order to have a fully integrated energy-harvesting system that includes both energy generation and storage, it is necessary to understand the dynamics of the leakage of the induced charge. The charge accumulation at the electrode surfaces will remain until the polarization field in the PPFE decays, or until a discharge path is created. In the present work, we focus on the characterization for metallic and also CNTF-based electrodes since the latter has been proposed as a potential material for supercapacitors to be integrated with FENG devices.⁷

The mechanical input in the following study was a step signal, where a pressure is applied and sustained on the device, while $V_{\rm OC}$ is monitored. Similar to the cyclic mechanical input, a single mechanical step also induces charge in the electrodes and generates an electric field during the compression cycle (stage 1 in Figure 3); however, the generated electric potential (i.e., $V_{\rm OC}$) is held until the generated displacement field decays due to dipole relaxation, or the charge is leaked through parasitic elements (stage 2 in Figure 3), which could be through a resistive load, the internal resistance of the voltmeter used to measure $V_{\rm OC}$, or through the input impedance of a power management circuit connected between the FENG device and an energy storage unit. In both discharging processes, charge flows in the same direction, but they do not necessarily have to flow at the same rate. Identifying the faster mechanism will shed light on the dominant discharging process in FENG devices, and this information is crucial at the time of designing voltage regulators that will connect the device (as an energy harvester) with an integrated energy storage system, e.g., a supercapacitor.

Before analyzing the results, it is important to note that $V_{\rm OC}$ measurements (particularly their dynamic behavior) are influenced by the internal resistance of the instrument used. 41 $V_{\rm OC}$ measurements get closer to the the real $V_{\rm OC}$ as the internal impedance of the instrument used increases. This means that the individual lumped parameters obtained for each device in the work described next may be different from the ideal scenario where an ideal voltmeter (with $R_{\rm inst} = \infty$) is used, but the qualitative comparisons and conclusions should still hold. In the present study, the same, high impedance voltmeter (Keithley 2450 Source Measure Unit, $R_{\rm inst} = 10~{\rm G}\Omega$) was used for all experiments.

Figure 4 shows sample curves for the mechanical step input experiment; a complete list of all the measurement results can be found in the Supporting Information. The experiment was repeated three times for each sample at each pressure, and the results consistently show that longest discharging times are for the silver-based electrodes and the shortest time is for the CNTF-A sample (see Figure 5). Faster discharging times were found when using other instruments with lower $R_{\rm inst}$.

It was found that dipole relaxation is not the faster mechanism for the discharging of the dipole-generated charge at each surface after the step input. The experiment that confirmed this consisted connecting a switch (normally open) between one of the measuring instrument terminals and a device electrode. In a sequence of separate experiments, the switch was closed at increasing times after applying the mechanical input, until no electric potential was measured (i.e.,

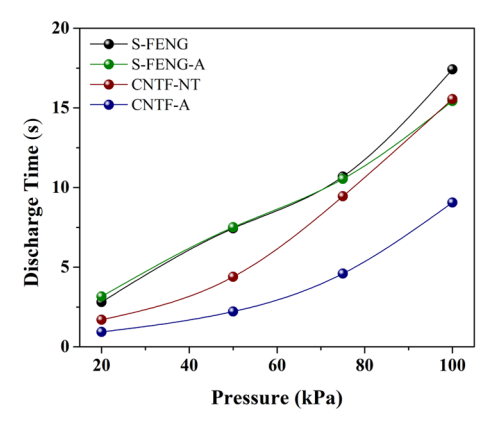


Figure 5. Discharge time for the four samples as a function of applied pressure. The total time represents the combination of dipole relaxation and leakage current processes.

 $V_{\rm OC}=0$). By having an open switch between the electrode and the measuring instrument, the induced charge does not have an electrical discharge path, leaving the relaxation of the dipoles (and consequently decrease of the dipole field) as the only charge leak mechanism. It was found that the voltage reading after closing the switch was different than zero for up to 180 s, which is more than 7 times higher than the total discharge time measured for any sample at any pressure (Figure 5). Thus, if the dipole-induced charge generated by FENG devices is to be stored, the discharging rate that needs to be considered is the one due to leakage through parasitic elements or the input impedance of the energy storage unit.

This current leakage was found to be the slowest for the two silver-based electrodes and fastest for the CNTF-A sample. This indicates that the reduction in $d_{\rm PPFE}$ due to acetone treatment does not dominate the leakage discharging time for any of the tested pressures since S-FENG-A also has a reduced $d_{\rm PPFE}$ but shows larger current discharge times. The faster responses for the two CNTF-based electrodes suggest that discharge times decrease with electrode resistivity.

2.4. Electrode Reliability. In addition to understanding the behavior of CNTFs as FENG electrodes to assist in their integration with monolithically integrated energy storage systems, another motivation for this work is to increase reliability and robustness of FENG devices. To that end, we proceeded to compare the response of S-FENG and CNTF samples after being subjected to wear and folding. One of the S-FENG samples was folded twice, while the other was submitted to a crumpling process that consisted of multiple random folds of different magnitudes and in different directions (see Figure 6). Electrical measurements showed that the S-FENG output was not affected significantly by folding, but no output was measured on the samples that were crumpled. Microcracks were visible to the naked eye in the silver electrodes on both samples. Such cracks were not noticed on the CNTF samples, which showed similar output after folding and crumpling. This confirms that more reliable and robust electrodes in FENG devices can be obtained by replacing metallic electrodes with CNT fibers.

3. CONCLUSIONS

The present work presents a step forward toward the development of monolithically integrated, flexible, robust ferroelectret energy-harvesting systems. The focus is at the electrode interface, where brittle, nonflexible metals have

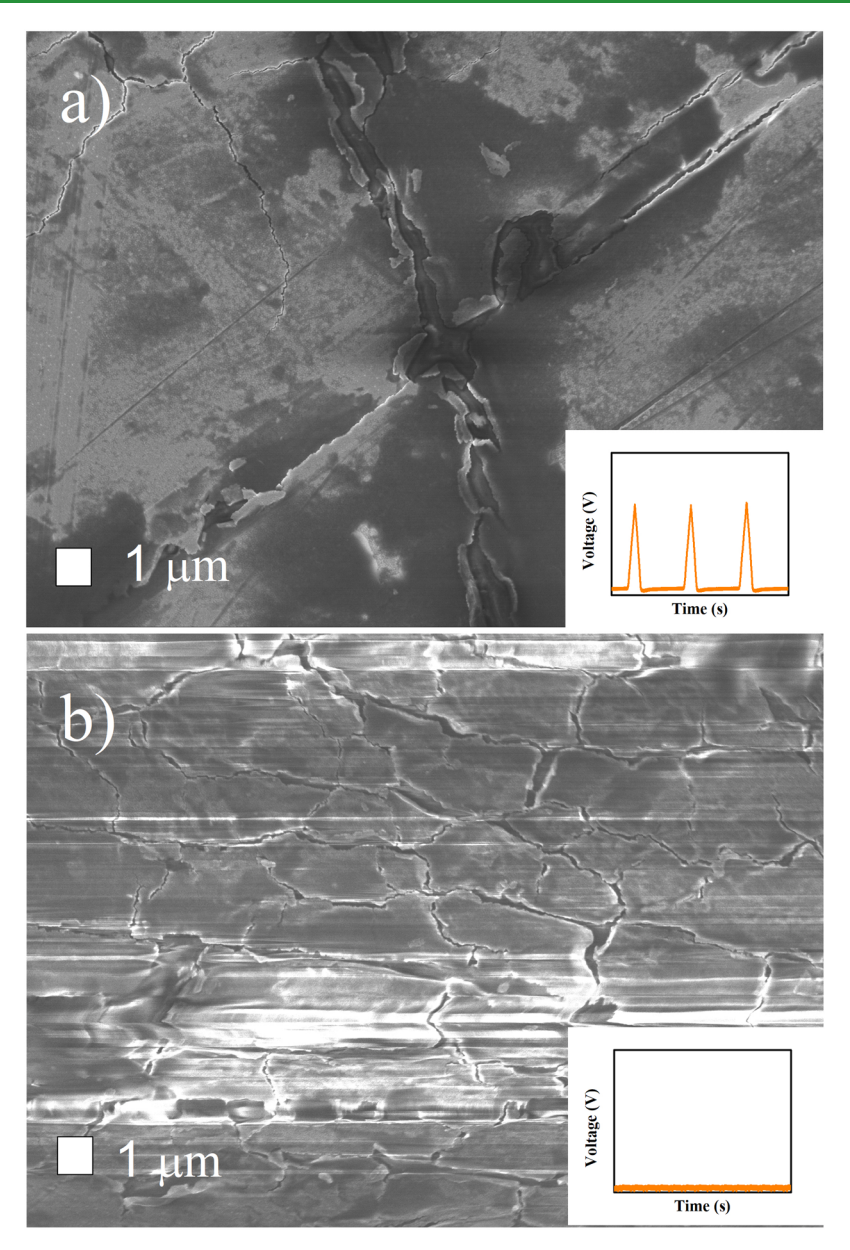


Figure 6. SEM images of S-FENG (a) after folding and (b) after crumpling. Inset plots show the electrical output in each case: there is still some electrical output after folding, but no output is observed after crumpling. CNTF-based electrode samples maintained the same electrical output in both cases.

traditionally been the material of choice and are replaced in the present work with CNTFs. The study includes the effects of acetone treatment on the CNTF-based electrodes and on the PPFE. The performance of these samples was compared to that of their metal-based electrode counterparts. Both $V_{\rm OC}$ and $I_{\rm SC}$ have been characterized as a function of pressure. Although CNTFs are much thicker and have a higher elastic modulus than thin metal films commonly used as electrodes, it was found that electrode conductivity was the dominant parameter in the generation/accumulation of free charge at the electrode surface. However, it was not clear that this mechanism dominated $I_{\rm SC}$ since this parameter did not show a large difference between the silver and CNTF-NT samples.

4. EXPERIMENTAL SECTION

4.1. Fabrication of FENG Devices. In order to study and compare the effects of different electrodes (and their processing) on

the electrical output of FENGs, three devices with distinct electrodes were prepared: (1) silver electrodes (S-FENG), (2) CNT fibers (CNTF-NT), and (3) CNT fibers treated with acetone (CNTF-A). The silver electrodes consisted of a thin film deposited over the polypropylene (~500 nm) using a sputter coater (Hummer X, Anatech Inc.). Electrical wires were manually attached to each electrode using conductive copper tape for output connections. Since the samples were submitted through various compressing/decompressing cycles, Kapton tape (poly-oxydiphenylene-pyromellitimide) was used to encapsulate the samples to prevent any deterioration from extensive and consecutive electrical characterization. The PPFE used for all samples was ordered from EMFIT Corporation. The fabrication of each device is discussed next and shown in Figure 7.

4.1.1. S-FENG. Figure 7a shows the fabrication process. A sputter coater (Hummer X, Anatech Inc.) was used to deposit a thin film of silver (~500 nm) over both sides of a polypropylene foam (area of 20 mm × 40 mm) (Figure 7a2). Electrical wires were manually attached to each electrode using copper tape (Figure 7a3). Finally, Kapton tape was used to encapsulate the sample (Figure 7a4).

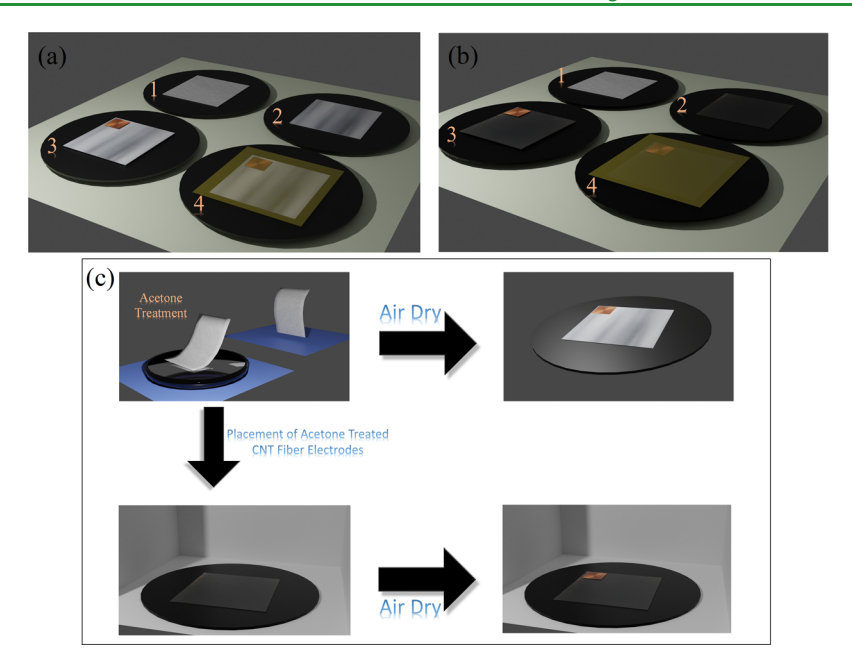


Figure 7. Sample fabrication process of (a) S-FENG, (b) CNTF-NT, and (c) CNTF-A and S-FENG-A samples.

4.1.2. CNTF-NT. Figure 7b shows the fabrication process. The fabrication and characterization of the carbon nanotube (CNT) fiber are discussed in detail elsewhere \$\frac{8}{12},13\$ In brief, CNT fiber samples consisted of unidirectional fabrics of multiple overlaid CNT fiber filaments, produced by spinning directly from the gas phase during CNT growth by chemical vapor deposition. The volumetric fraction for the CNTF-NT samples was around 0.512. Electrical wires were connected similarly to the S-FENG sample (Figure 7b3). The process was followed by placing Kapton tape over the fiber, trying to avoid electrical discontinuity or additional mechanical wrinkling of the fiber by carefully placing the tape and placing it over the fiber. The tape was lifted with the fiber and then placed over the surface of the polypropylene foam (Figure 7b4).

The CNT fiber is predominantly made up of multiwalled CNTs (MWCNTs) with an average outer diameter of 5 nm and three layers, as reported previously, 44 making it a complex hierarchical structure. At the smallest scale, the fiber is made up of few-layer MWCNTs. They are associated into bundles, somewhat analogous to elongated graphitic crystals, where the CNTs are in close proximity under turbostratic stacking. The macroscopic fibers or CNT fiber layers are macroscopic networks formed by continuous bundles. The axial elastic modulus of the constituent MWCNT is in the range of 1 TPa. In the CNT fiber, the MWCNTs are predominantly aligned in the layer direction but randomly oriented in the plane. The longitudinal modulus of the densified CNT fiber layer is around 10 GPa.

4.1.3. CNTF-A. The CNT fiber and the PPFE foam were submerged in a Petri dish with acetone (Figure 7c). To attach the second electrode, a visually transparent substrate was used to cover the side; the first electrode was already placed in order to monitor the electrode while removing the substrate. This process fixed the electrode, preventing it from detaching or moving from its intended position. The sample was left drying for 3 min. Finally, electrical wires were attached and the sample was encapsulated in Kapton tape. The volumetric fraction for the CNTF-A samples was around 0.272.

Dimensions for the silver and CNTF-NT electrodes devices were 20 mm × 40 mm. The CNTF-A sample was cut with these dimensions also, but upon acetone exposure, the fiber wrinkled in both lateral and longitudinal directions. Stretching of the fiber was done immediately after it was placed over the foam, taking advantage the fiber was still wet and allowed easier manipulation. However, despite this effort, the final size of the CNTF-A sample was slightly smaller. The volumetric fractions given for the CNTF-NT and CNTF-A samples are extracted directly from image analysis of

electron micrographs in the following section, corresponding to the apparent density. More accurate determination of the density of the CNT fiber layer poses the question as to which density to take among: the apparent density, skeletal density (without open pores), or density with respect to graphite single crystal. ⁴⁵ Furthermore, we note that the areal density (i.e., mass per unit length) of the CNT fiber is the same, and that for both samples, there is extensive contact between the polymer phase and the current collector.

4.2. Scanning Electron Microscopy (SEM) Characterization. SEM micrographs were obtained using a JEOL 7500F field emission emitter scanning electron microscope (JEOL Ltd., Tokyo, Japan.) operated at 5 kV. Figure 8a,c shows top view and cross section of the

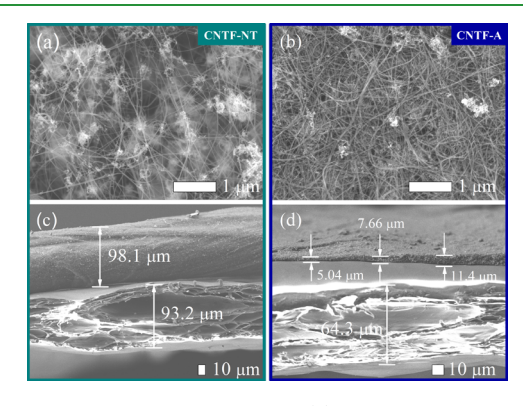


Figure 8. SEM pictures of CNT fiber (a) with no acetone treatment (CNTF-NT) and (b) with acetone treatment (CNTF-A). The higher density and packing fraction of the CNTF-A film can be noticed. Cross-sectional views for (c) CNTF-NT and (d) CNTF-A.

carbon nanotube fiber without acetone treatment, respectively. It is clear from the top view that the fiber density is lower for the sample with no acetone treatment. The thickness for the fiber with no acetone treatment is 98 $\mu \rm m$. In contrast, Figure 8b,d shows how the acetone treatment decreases the air voids, increasing the fiber's density and the contact between individual CNT fibers. In addition, the fiber's thickness decreases by a factor of 10. It can also be seen from the SEM image how the thickness becomes nonuniform. Finally, acetone treatment on the polypropylene also had the same shrinking effect. In this case, it was reduced by 30 $\mu \rm m$ when treated with acetone.

ASSOCIATED CONTENT

Supporting Information

The Supporting Information is available free of charge at https://pubs.acs.org/doi/10.1021/acsami.0c02019.

Measurement setup, derivation of eq 1 on the manuscript, and tables with average values taken from all the experimental runs done to characterize the devices (PDF)

AUTHOR INFORMATION

Corresponding Author

Nelson Sepúlveda - Department of Electrical and Computer Engineering, Michigan State University, East Lansing, Michigan 48824, United States; o orcid.org/0000-0002-9676-8529; Email: nelsons@egr.msu.edu

Authors

- Juan Pastrana Department of Electrical and Computer Engineering, Michigan State University, East Lansing, Michigan 48824, United States
- Henry Dsouza Department of Electrical and Computer Engineering, Michigan State University, East Lansing, Michigan 48824, United States
- Yunqi Cao Ming Hsieh Department of Electrical and Computer Engineering - Electrophysics, University of Souther California, Los Angeles, California 90007, United States
- José Figueroa Department of Electrical and Computer Engineering, Michigan State University, East Lansing, Michigan 48824, United States
- Ian González Department of Electrical and Computer Engineering, Michigan State University, East Lansing, Michigan 48824, United States
- Juan J. Vilatela IMDEA Materials Institute, 28906 Getafe, Madrid, Spain; orcid.org/0000-0002-2572-0245

Complete contact information is available at: https://pubs.acs.org/10.1021/acsami.0c02019

The authors declare no competing financial interest.

ACKNOWLEDGMENTS

This work was supported by the National Science Foundation (NSF ECCS Award: ECCS-1854750).

REFERENCES

- (1) Zhan, Z.; Lin, R.; Tran, V.-T.; An, J.; Wei, Y.; Du, H.; Tran, T.; Lu, W. Paper/Carbon Nanotube-Based Wearable Pressure Sensor for Physiological Signal Acquisition and Soft Robotic Skin. ACS Appl. Mater. Interfaces 2017, 9, 37921-37928.
- (2) Schwartz, G.; Tee, B. C.-K.; Mei, J.; Appleton, A. L.; Kim, D. H.; Wang, H.; Bao, Z. Flexible Polymer Transistors with High Pressure Sensitivity for Application in Electronic Skin and Health Monitoring. Nat. Commun. 2013, 4, 1859-1866.
- (3) Askari, H.; Hashemi, E.; Khajepour, A.; Khamesee, M. B.; Wang, Z. L. Towards Self-powered Sensing Using Nanogenerators for Automotive Systems. Nano Energy 2018, 53, 1003-1019.
- (4) Presas, A.; Luo, Y.; Wang, Z.; Valentin, D.; Egusquiza, M. A Review of PZT Patches Applications in Submerged Systems. Sensors 2018, 18, 2251-2272.
- (5) Boukabache, H.; Escriba, C.; Fourniols, J.-Y. Toward Smart Aerospace Structures: Design of a Piezoelectric Sensor and its Analog Interface for Flaw Detection. Sensors 2014, 14, 20543-20561.

- (6) Deng, H.; Du, Y.; Wang, Z.; Ye, J.; Zhang, J.; Ma, M.; Zhong, X. Poly-stable Energy Harvesting Based on Synergetic Multistable Vibration. Commun. Phys. 2019, 2, 21-30.
- (7) Yong, S.; Shi, J.; Beeby, S. Wearable Textile Power Module Based on Flexible Ferroelectret and Supercapacitor. Energy Technol. 2019, 7, 1800938-1800959.
- (8) Koziol, K.; Vilatela, J.; Moisala, A.; Motta, M.; Cunniff, P.; Sennett, M.; Windle, A. High-performance Carbon Nanotube Fiber. Science 2007, 318, 1892-1895.
- (9) Vilatela, J. J.; Marcilla, R. Tough Electrodes: Carbon Nanotube Fibers as the Ultimate Current Collectors/active Material for Energy Management Devices. Chem. Mater. 2015, 27, 6901-6917.
- (10) Lim, J.; Knabe, K.; Tillman, K. A.; Neely, W.; Wang, Y.; Amezcua-Correa, R.; Couny, F.; Light, P. S.; Benabid, F.; Knight, J. C.; Corwin, K. L.; Nicholson, J. W.; Washburn, B. R. A Phasestabilized Carbon Nanotube Fiber Laser Frequency Comb. Opt. Express 2009, 17, 14115-14120.
- (11) Choi, J.; Jung, Y.; Yang, S. J.; Oh, J. Y.; Oh, J.; Jo, K.; Son, J. G.; Moon, S. E.; Park, C. R.; Kim, H. Flexible and Robust Thermoelectric Generators Based on All-Carbon Nanotube Yarn without Metal Electrodes. ACS Nano 2017, 11, 7608-7614.
- (12) Senokos, E.; Reguero, V.; Cabana, L.; Palma, J.; Marcilla, R.; Vilatela, J. J. Large-Area, All-Solid, and Flexible Electric Double Layer Capacitors Based on CNT Fiber Electrodes and Polymer Electrolytes. Adv. Mater. Technol. 2017, 2, 1600290.
- (13) Senokos, E.; Ou, Y.; Torres, J. J.; Sket, F.; González, C.; Marcilla, R.; Vilatela, J. J. Energy Storage in Structural Composites by Introducing CNT Fiber/polymer Electrolyte Interleaves. Sci. Rep. 2018, 8, 3407.
- (14) Jiang, H.; Lee, P. S.; Li, C. 3D Carbon Based Nanostructures for Advanced Supercapacitors. Energy Environ. Sci. 2013, 6, 41-53.
- (15) Wang, Y.; Wei, H.; Lu, Y.; Wei, S.; Wujcik, E.; Guo, Z. Multifunctional Carbon Nanostructures for Advanced Energy Storage Applications. Nanomaterials 2015, 5, 755-777.
- (16) Bauer, S. Piezo-, Pyro- and Ferroelectrets: Soft Transducer Materials for Electromechanical Energy Conversion. IEEE Trans. Dielectr. Electr. Insul. 2006, 13, 953-962.
- (17) Bauer, S.; Gerhard-Multhaupt, R.; Sessler, G. M. Ferroelectrets : Soft Electroactive Foams for Transducers. Phys. Today 2004, 57,
- (18) Paajanen, M.; Wegener, M.; Gerhard-Multhaupt, R. Understanding the Role of the Gas in the Voids During Corona Charging of Cellular Electret Films - A Way to Enhance Their Piezoelectricity. J. Phys. D: Appl.Phys. 2001, 34, 2482-2488.
- (19) Wang, T.; Farajollahi, M.; Choi, Y. S.; Lin, I.-T.; Marshall, J. E.; Thompson, N. M.; Kar-Narayan, S.; Madden, J. D. W.; Smoukov, S. K. Electroactive Polymers for Sensing. Interface focus 2016, 6, 20160026.
- (20) Wang, B.; Liu, C.; Xiao, Y.; Zhong, J.; Li, W.; Cheng, Y.; Hu, B.; Huang, L.; Zhou, J. Ultrasensitive Cellular Fluorocarbon Piezoelectret Pressure Sensor for Self-powered Human Physiological Monitoring. Nano Energy 2017, 32, 42-49.
- (21) Li, W.; Torres, D.; Wang, T.; Wang, C.; Sepúlveda, N. Flexible and Biocompatible Polypropylene Ferroelectret Nanogenerator (FENG): On the Path Toward Wearable Devices Powered by Human Motion. Nano Energy 2016, 30, 649-657.
- (22) Zhang, X.; Pondrom, P.; Sessler, G. M.; Ma, X. Ferroelectret Nanogenerator with Large Transverse Piezoelectric Activity. Nano Energy 2018, 50, 52-61.
- (23) Shi, J.; Yong, S.; Beeby, S. An Easy to Assemble Ferroelectret for Human Body Energy Harvesting. Smart Mater. Struct. 2018, 27, No. 084005.
- (24) Zhang, X.; Sessler, G. M.; Wang, Y. Fluoroethylenepropylene Ferroelectret Films with Cross-tunnel Structure for Piezoelectric Transducers and Micro Energy Harvesters. J. Appl. Phys. 2014, 116, No. 074109
- (25) Wang, Y.; Wu, L.; Zhang, X. Energy Harvesting from Vibration using Flexible Floroethylenepropylene Piezoelectret Films with Cross-

I

- tunnel Structure. IEEE Trans. Dielectr. Electr. Insul. 2015, 22, 1349—1354.
- (26) Li, X.; Lin, Z.-H.; Cheng, G.; Wen, X.; Liu, Y.; Niu, S.; Wang, Z. L. 3D Fiber-Based Hybrid Nanogenerator for Energy Harvesting and as a Self-Powered Pressure Sensor. *ACS Nano* **2014**, *8*, 10674–10681.
- (27) Lu, Z.; Raad, R.; Safaei, F.; Xi, J.; Liu, Z.; Foroughi, J. Carbon Nanotube Based Fiber Supercapacitor as Wearable Energy Storage. *Front. Mater.* **2019**, *6*, 138.
- (28) Shepelin, N. A.; Glushenkov, A. M.; Lussini, V. C.; Fox, P. J.; Dicinoski, G. W.; Shapter, J. G.; Ellis, A. V. New Developments in Composites, Copolymer Technologies and Processing Techniques for Flexible Fluoropolymer Piezoelectric Generators for Efficient Energy Harvesting. *Energy Environ. Sci.* 2019, 12, 1143–1176.
- (29) Zohair, M.; Moyer, K.; Eaves-Rathert, J.; Meng, C.; Waugh, J.; Pint, C. L. Continuous Energy Harvesting and Motion Sensing from Flexible Electrochemical Nanogenerators: Toward Smart and Multifunctional Textiles. *ACS Nano* **2020**, *14*, 2308–2315.
- (30) Sundaram, R. M.; Windle, A. H. One-step Purification of Direct-spun CNT Fibers by Post-production Sonication. *Mater. Des.* **2017**, *126*, 85–90.
- (31) Liu, K.; Sun, Y.; Zhou, R.; Zhu, H.; Wang, J.; Liu, L.; Fan, S.; Jiang, K. Carbon Nanotube Yarns with High Tensile Strength Made by a Twisting and Shrinking Method. *Nanotechnology* **2009**, *21*, No. 045708.
- (32) Kang, D.; Pikhitsa, P. V.; Choi, Y. W.; Lee, C.; Shin, S. S.; Piao, L.; Park, B.; Suh, K.-Y.; Kim, T.-I.; Choi, M. Ultrasensitive Mechanical Crack-based Sensor Inspired by the Spider Sensory System. *Nature* **2014**, *516*, 222.
- (33) Kim, S. M.; Ahn, C.-Y.; Cho, Y.-H.; Kim, S.; Hwang, W.; Jang, S.; Shin, S.; Lee, G.; Sung, Y.-E.; Choi, M. High-performance Fuel Cell with Stretched Catalyst-Coated Membrane: One-step Formation of Cracked Electrode. *Sci. Rep.* **2016**, *6*, 26503.
- (34) Wang, H.; Shi, M.; Zhu, K.; Su, Z.; Cheng, X.; Song, Y.; Chen, X.; Liao, Z.; Zhang, M.; Zhang, H. High Performance Triboelectric Nanogenerators with Aligned Carbon Nanotubes. *Nanoscale* **2016**, *8*, 18489–18494.
- (35) Khan, S. A.; Zhang, H. L.; Xie, Y.; Gao, M.; Shah, M. A.; Qadir, A.; Lin, Y. Flexible Triboelectric Nanogenerator Based on Carbon Nanotubes for Self-Powered Weighing? *Adv. Eng. Mater.* **2017**, *19*, 1600710.
- (36) Xiong, J.; Lee, P. S. Progress on Wearable Triboelectric Nanogenerators in Shapes of Fiber, Yarn, and Textile. *Sci. Technol. Adv. Mater.* **2019**, *20*, 837–857.
- (37) Zhong, J.; Zhang, Y.; Zhong, Q.; Hu, Q.; Hu, B.; Wang, Z. L.; Zhou, J. Fiber-Based Generator for Wearable Electronics and Mobile Medication. *ACS Nano* **2014**, *8*, 6273–6280.
- (38) Cao, Y.; Figueroa, J.; Pastrana, J. J.; Li, W.; Chen, Z.; Wang, Z. L.; Sepúlveda, N. Flexible Ferroelectret Polymer for Self-Powering Devices and Energy Storage Systems. ACS Appl. Mater. Interfaces 2019, 11, 17400–17409.
- (39) Qiu, J.; Terrones, J.; Vilatela, J. J.; Vickers, M. E.; Elliott, J. A.; Windle, A. H. Liquid Infiltration Into Carbon Nanotube Fibers: Effect on Structure and Electrical Properties. *ACS Nano* **2013**, *7*, 8412–8422.
- (40) Li, Y.; Lu, W.; Sockalingam, S.; Gu, B.; Sun, B.; Gillespie, J. W.; Chou, T.-W. Electromechanical Behavior of Carbon Nanotube Fibers Under Transverse Compression. *J. Phys. D: Appl. Phys.* **2017**, *50*, No. 085303.
- (41) Cao, Y.; Figueroa, J.; Li, W.; Chen, Z.; Wang, Z. L.; Sepúlveda, N. Understanding the Dynamic Response in Ferroelectret Nanogenerators to Enable Self-powered Tactile Systems and Human-controlled Micro-robots. *Nano Energy* **2019**, *63*, 103852.
- (42) Luo, Z.; Zhu, D.; Beeby, S. An Electromechanical Model of Ferroelectret for Energy Harvesting. *Smart Mater. Struct.* **2016**, 25, No. 045010.
- (43) Wang, Z. L. On Maxwell's Displacement Current for Energy and Sensors: The Origin of Nanogenerators. *Mater. Today* **2017**, *20*, 74–82.

- (44) Reguero, V.; Alemán, B.; Mas, B.; Vilatela, J. J. Controlling Carbon Nanotube Type in Macroscopic Fibers Synthesized by the Direct Spinning Process. *Chem. Mater.* **2014**, *26*, 3550–3557.
- (45) Santos, C.; Senokos, E.; Fernández-Toribio, J. C.; Ridruejo, Á.; Marcilla, R.; Vilatela, J. J. Pore structure and electrochemical properties of CNT-based electrodes studied byin situsmall/wide angle X-ray scattering. *J. Mater. Chem. A* **2019**, *7*, 5305–5314.